Soft Matter

Accepted Manuscript

ROYAL SOCIETY OF CHEMISTRY

www.rsc.org/softmatter

Semi-crystalline polymethylene-*b*-poly(acrylic acid) diblock copolymers: aggregation behavior, confined crystallization and controlled growth of semicrystalline micelles from dilute DMF solution†

Hongfang Wang[a], Cong Wu[a], Guangmei Xia[b], Zhi Ma[c], Guang Mo[d], Rui Song*[a]

[a]*College of Chemistry and Chemical Engineering, University of Chinese Academy of Sciences,Beijing 100049, China*

[b]*Beijing National Laboratory for Molecular Sciences, CAS Key Laboratory of Engineering Plastics, Institute of Chemistry, Chinese Academy of Sciences, Beijing 100190, China*

[c]*Shanghai Institute of Organic Chemistry, Chinese Academy of Sciences, Shanghai 200032, China*

[d]*Beijing Synchrotron Radiation Facility (BSRF), Institute of High Energy Physics, Chinese Academy of Sciences Beijing, 100049, China*

Abstract: In this paper, we have systematically investigated the aggregation behavior, confined crystallization and controlled growth of a novel polyolefin analogue-containing block copolymers (BCPs), *i.e*., polymethylene-*b*-poly(acrylic acid) diblock copolymers (PM-*b*-PAA). Cooling from a homogenous DMF solution at 80 °C, PM-*b*-PAA was found to crystallize and aggregate with well-defined disk-like micelles. Besides, the aggregate behavior and in-plane morphology of PM-*b*-PAA could be facilely controlled by block ratio, solution pH value and solvent composition (DMF-water), via manipulating the crystallization of PM block and the stretching degree of solvated PAA corona. Further probe on the crystalline feature of PM-*b*-PAA indicated that the crystallization of PM was retarded by tethered amorphous PAA segment. The crystalline micelle could construct a nanoconfined environment with PM folding as the core into a thickness of the mono-layered polyethylene. Finally, when cultured in dilute DMF solution at 50 °C, the initial crystalline micelles, being as self-seeds, could follow a living growth mechanism and develop into single crystals, even with well-defined lozenge-shaped morphology.

Introduction

In recent decades, much attention has been attracted to the block copolymers (BCPs), which can self assemble into various morphologies including sphere, cylinder, and lamellae due to the inherent immiscibility of different polymer segments.[1,2] Besides their abundant ordered morphologies in nanoscale, BCPs, especially the "crew-cut" BCPs reported by Eisenberg *et al*,[1,3] can manipulate their overall architectures *via* altering the block composition and processing conditions. Hence, BCPs were widely used in lithography,[4] drug delivery,[5] and optoelectronic devices,[6] *etc.*

Different from the conventional coil-coil block copolymers, semi-crystalline BCPs, which comprise at least one crystallizable block, are attracting increasing awareness due to their significance to theoretical research and potential applications.[7, 8] In the simplest case, semi-crystalline BCPs can increase morphological richness with the crystallization as another driving force. Previous works on crystalline-coil BCPs have proved that anisotropic morphologies such as cylinder,[9,10] long worm-like,[11] multicores,[12] disk-like,[13] concentric lenticular[14], and some other complex nanostructures are readily available due to the chain-folding of crystalline segment or the crystallization driven self-assembly (CDSA)[10,14]. Yet, it is relatively complicate to obtain these structures for amorphous BCPs, which usually require solvent inducement and dialysis.[1] In fact, acquisition and regulation of the asymmetry morphologies are of great importance. For example, long worm-like poly(ε-caprolactone)-*b*-poly(ethylene oxide) (PCL-*b*-PEO) micelles show improved performance in drug delivery than spherical micelles.[15] Besides, crystalline-coil BCPs can be applied to construct a nanoconfined environment with polymer crystals in thickness comparable to the size of microdomains induced by microphase separation.[16, 17]

Previous researches on the crystalline BCPs have found that when cooled from a high temperature (usually close to the melting temperature of the crystalline block) in coil-selective solution, BCPs were inclined to crystallize and formed disk-like crystalline micelles with semi-crystalline chain folding as core and the chemically tethered amorphous block swelling as corona. This aggregate structure was predicted

with the scale law put forward by Vilgis *et al.*[18] and have been widely observed in semi-crystalline BCPs that containing crystallizable block like polyethylene (PE),[19-22] poly(ethylene oxide (PEO),[23] poly(ε-caprolactone) (PCL),[24] *etc.* Except the disk-like or platelet crystalline micelles, other types of architectures such as spheres, rods, worm-like nanostructures, and the manipulation techniques, *e.g.*, adjusting block composition, temperature and solution pH value, have also been investigated.[25-28] In addition, research attention has also been paid to the controlled growth of crystalline micelles by regulating the crystallization process to achieve crystal plates or single crystals.[29-31] However, to the best of our knowledge, acquisition of single crystal in semi-crystalline BCPs is seldomly reported.[30] And the aggregation behavior for crystalline-containing BCPs micelles in dilute solution, especially the controlling methods are not well established.[24]

Herein, a novel polyolefin analogue-containing BCPs, *i.e.,* polymethylene-*b*-poly (acrylic acid) diblock copolymers (PM-*b*-PAA) were selected to discuss the aggregation behavior and controlled growth of semi-crystalline BCPs. The structure of PM is identical to that of polyethylene, which is easy to crystallize with the flexible and regular chain. Detailed effects of block composition, solvent quality, and solution pH value on the aggregate behaviors of PM-*b*-PAA in DMF or aqueous solution were systematically investigated by atomic force microscopy (AFM), transmission electron microscopy (TEM) and dynamic light scattering (DLS). Moreover, confined crystallization of the PM-*b*-PAA and its controlled growth in dilute DMF solution were studied with measurements of differential scanning calorimetry (DSC), grazing-incidence x-ray diffraction (GIXRD), TEM and high resolution TEM (HRTEM), *etc*.

2. Experimental Section:

2.1 Chemicals and Materials

Block copolymers (BCPs), polymethylene-*b*-poly(acrylic acid) were kindly supplied from Prof. Zhi Ma, Shanghai Institute of Organic Chemistry, Chinese Academy of Sciences. Details about their synthesis and structure characterization can

be found elsewhere.[32] Number-average molecular weight (M_n), polydispersity index (M_w/M_n), crystallization temperature (T_c) and melting temperature (T_m) of all the samples are listed in **Table 1**. N, N-dimethylformamide (DMF), Sinopharm Chemical Reagent Co. Ltd., was distilled before use. Deionized (DI) water (18.2 MΩ cm) was produced by ultrapure water systems (Ulupure Co. Ltd., Shanghai, China).

Table 1 Summary of some characteristic parameters for PM-*b*-PAA bulk samples

Sample[a]	M_n [g mol^{-1}]	M_w/M_n	PM [mol%]	T_c [b] [°C]	T_m [b] [°C]
$\mathbf{M_{93}A_{94}}$	8800	1.10	50.53	66.3	79.6
$\mathbf{M_{214}A_{81}}$	8100	1.09	72.54	85.8	96.7
$\mathbf{M_{107}A_5}$	1900	1.09	95.53	81.6	108.1

[a] The subscript numbers denote the number-average degree of polymerization. [b] Phase transition temperature was traced by DSC thermogram at heating and cooling rate of 10 °C min^{-1}.

Silicon wafers {100}, about 1×1 cm^2 were used as substrates for atomic force microscopy (AFM). Grazing-incidence small-angle x-ray scattering (GISAXS) and grazing-incidence x-ray diffraction (GIXRD) characterization. Before use, the silicon wafers were cleaned by acetone (30 min), DI water (10 min), H_2O_2 (30 min), and piranha solution (4:1 v/v H_2SO_4/H_2O_2, 15 min) in sequence. After rinsed with DI water, the substrates were further cleaned by $H_2O_2/NH_3/H_2O$ (1:1:1 v/v, 15 min) solution and dried on a hot plate at a temperature above 200 °C.

2.2 Preparation of the semi-crystalline micellar solution with different conditions

Typically, 2 mg of PM-*b*-PAA was ultrasonically dispersed in 10 mL of DMF or ultrapure water at room temperature. Then, the solution was heated to 80 °C, which was close to the melting temperature (T_m) of PM (see **Table 1**) since it is difficult for nonpolar crystalline polyolefin-contained BCPs to dissolve at room temperature.[33-35] The solution was stirred at 80 °C for 30 min followed by cooling down to room temperature at a rate of ~0.5 °C min^{-1}, and stirred for another 24 h at ambient

condition. Finally, a homogeneous solution with a concentration of 0.2 mg mL^{-1} was obtained for further analysis.

To clarify the effect of block composition on the aggregation behavior of PM-*b*-PAA, different types of PM-*b*-PAA samples in DMF were prepared for comparison. And to explore the influence of the solvent quality on the aggregate structures of PM-*b*-PAA, a predetermined amount of BCPs aqueous solution was dropwisely added to the BCPs/DMF solution, accompanied with vigorously shaking. Then, the mixture with different water contents (x % = 0, 20, 30, 50 vol %.) was stirred for 24 h to obtain a homogeneous BCPs solution with a concentration of 0.2 mg mL^{-1}.

Furthermore, in order to explore the influence of solution pH value on the aggregation of PM-*b*-PAA, PM-*b*-PAA aqueous solution with desired pH value (2, 5, 7, 9, 12) was prepared by dropwisely adding a small amount of HCl or NaOH aqueous solution (2 mol L^{-1} and 0.2 mol L^{-1}) into the as-prepared 0.2 mg mL^{-1} aqueous solution without bringing distinct change in solution volume. And the final micellar solutions were used for further characterization.

2.3 Controlled growth from dilute BCPs/DMF solution

BCPs/DMF (0.2 mg mL^{-1}) solution was stirred for 4 h under 120 °C, a temperature well above the melting temperature of PE segment, to form a homogeneous solution. Then, the solution was allowed to stand still and slowly cooled to 50 °C at a rate of ~0.5 °C min^{-1}. Finally, the sample was kept at 50 °C to follow the crystal growth process.

3. Results and Discussion

3.1 Aggregation behavior of PM-*b*-PAA and its influential factors

Herein, DMF or water, a good solvent for PAA was used for the preparation of PM-*b*-PAA aggregates with crystalline PM as core and solvated PAA as the corona by cooling the homogeneous solution from 80 °C. The final aggregate architectures were found to be controlled by factors like the block composition, solvent composition and solution pH value, and the detailed aggregate behavior as well as the mechanisms is

discussed as follows:

Effect of block composition on the aggregation behavior of PM-*b*-PAA

$\mathbf{M_{93}A_{94}}$ and $\mathbf{M_{214}A_{81}}$ with the similar degree of polymerization for PAA were chosen to study the effect of block composition on the subsequent aggregate morphology of PM-*b*-PAA. It is notable from the AFM images that the spin-coated $\mathbf{M_{93}A_{94}}$ samples (block ratio: PM/PAA $\approx$ 1:1) tend to form disk-like nanoaggregates with a spherical shape of ~30 nm in lateral dimension and ~7 nm in cross-section (**Fig. 1A**). Yet, when the block ratio for $\mathbf{M_{214}A_{81}}$ was raised to about 5:2 with PAA block length remaining close to $\mathbf{M_{93}A_{94}}$, BCPs were inclined to form spindle-like micelles with an average size of ~200 nm, ~30 nm and ~10 nm in three dimension, respectively (**Fig. 1B**). However, both of the AFM images suggested the aggregation of PM-*b*-PAA chain, since the micellar size is larger than the individual chain.[36] Besides, the anisotropic morphology of dried micelles, especially indicated from the apparent dimensional contrast between cross-section height and in-plane diameter, implied the aggregated platelet-like structure as had been reported for other crystalline-coil BCPs.[19] Furthermore, the thickness of ~10 nm for the micelles was in accordance with that of mono-layered polyethylene crystal, suggesting that PM block may crystallized into a single-layered plate similar as the crystallization of polyethylene in BCPs.[36]

The morphology transition along with different block compositions was further verified by TEM analysis with $\mathbf{M_{93}A_{94}}$ and $\mathbf{M_{214}A_{81}}$ samples being dropped on a copper grid from 0.2 mg mL^{-1} DMF solution. As shown in **Fig. 1C,** $\mathbf{M_{93}A_{94}}$ aggregated into micelles mainly with circular morphology in-plane and a lateral size of ~20 nm, which was mainly in accordance with the results of AFM in **Fig. 1A**. Besides, the existence of some rod-like cross-section with darker contrast (as indicated by the black circles in **Fig. 1C**) implied the crystalline component of the BCPs.[19] For the aggregates of $\mathbf{M_{214}A_{81}}$, a spindle-like morphology with an average length of ~150 nm revealed in **Fig. 1D** is also in accordance with the AFM results (**Fig. 1B**). The larger average size inspected by AFM than TEM can be probably

ascribed to the expansion effect of spin-coating method and the tip-broadening effect in AFM measurement.[23]

The aggregation behavior as a function of the block composition was believed to be determined by the competition between the folding degree of crystallizable block and the stretching degree of amorphous segment.[37,738] Indeed, it can be explained with the reduced tethering density $\tilde{\sigma}$ (see **Eq. 1**).[24, 39]

$$\tilde{\sigma} = \sigma \pi R_g^2 \qquad (1)$$

here σ is the tethered chain density and is equal to the reciprocal of the covered area of soluble chains (herein it refers to PAA chains), R_g is the radius of gyration of a free soluble block. In detail, when crystalline chain is the main component, the insoluble crystalline block tends to form more chain folds in the micellar core. Then, as the definition of $\tilde{\sigma}$ indicated, the value of $\tilde{\sigma}$ will reduce and morphologies with low interfacial curvature such as cylinders and platelets are favorable.[24] In the case of the $\mathbf{M_{214}A_{81}}$, the spindle shape, resulting from a larger degree of chain-folding in core-forming block, can be viewed as the intermediate morphology between cylinder and platelet. On the other hand, a relative long soluble chain favors the stretching of the corona block with a larger $\tilde{\sigma}$ involved. Namely, the amorphous chains are effectively covered around the folding surface and retard the fusion of semi-crystalline core. Therefore, spherical micelles were observed in $\mathbf{M_{93}A_{94}}$.

Effect of the solvent composition on the aggregation behavior of PM-*b*-PAA

The relationship between aggregation behavior of PM-*b*-PAA and solvent composition of water-DMF binary mixtures was revealed by the AFM and DLS results. Spin-coated from DMF solution, $\mathbf{M_{93}A_{94}}$ aggregated into spherical morphology with a uniform diameter of ~35 nm and a thickness of ~8 nm, as shown in the AFM height (**Fig. 2A**) and phase images (**Fig. 2A′**). However, an increasing content of water (20, 30, 50 vol %) in the system with the same BCPs concentration of 0.2 mg mL^{-1} would lead to the rod-like morphology in plane (**Fig. 2B-2D, 2B′-2D′)**.

Moreover, the average size of the aggregates increased to 200 nm together with a wide distribution, which was consistent with the corresponding variation in the hydrodynamic diameter, D_h, with the solvent quality as shown by DLS results (**Fig. 3)**. It should be noted that the cross-section height (~8 ± 3 nm) of the micelles was much smaller than the in-plane size, indicating the disk-like structures of the micelles as been mentioned above. In addition, the overall state of $\mathbf{M_{107}A_5}$ seemed to be more sensitive to the solvent environment than that of $\mathbf{M_{93}A_{94}}$, which possessed a more prominent morphology evolution with different water contents in the mixed solvent (**Fig. S1**).

The solvent environment was proved to control the morphology of BCPs, especially the "crew-cut" BCPs,[1] *via* altering the conformation of the block. For PM-*b*-PAA, both water and DMF are good solvent for PAA. However, as illustrated by the previous reports, the polyethylene block are insoluble in most solvent at room temperature. Nevertheless, the polymer-solvent interaction parameter $\chi_{\text{Polymer-Solvent}}$ (see **Eq. (2) (3)** and **Table 2**) for $\chi_{\text{PM-DMF}}$ (= 2.61) is smaller than $\chi_{\text{PM-H}_2\text{O}}$ (= 7.10), suggesting DMF is a relatively good solvent for PM block compared to water. Furthermore, a better dispersion for PM-*b*-PAA in DMF than in water in visual aspect could also illustrate this point. Therefore, increasing amount of the water could result in a relatively poor solvent for PM and then induce a higher surface tension in the core–solvent interface. As a result, the structural change from spherical micelles to larger aggregates with decreased interface between PM core and water was observed.

$$\chi = \chi_H + \chi_S \qquad (2)$$

$$\chi_H = \frac{V_1}{RT}(\delta_1 - \delta_2)^2 \qquad (3)$$

in these equations, χ_H is enthalpic contribution, χ_S is entropic contribution (usually is 0.34 for non-polar system[40]), V_1 is molar volume of the solvent, R is universal gas constant (= 8.314 J·K·mol^{-1}), δ_1, δ_2 are the Hildebrandt solubility parameters of ~~the~~

solvent and ~~the~~ polymer, respectively.

Table 2 The Hildebrandt solubility parameters δ and calculated polymethylene-solvent interaction parameters at T = 298 K.

Polymer	δ_2 [MPa $^{1/2}$]	Solvent	δ_1 [MPa $^{1/2}$]	V_1 [cm^3 mol^{-1}]	$\chi_{Polymer\text{-}Solvent}$
Polymethylene	16.2	DMF	12.1	77	2.61
Polymethylene	16.2	Water	23.2	18	7.10

The parameters of δ_1, δ_2, and V_1 are referred to handbook[41] and δ_1 was referred to that of polyethylene.

Effect of solution pH value on the aggregation behavior of PM-*b*-PAA

In order to determine whether the aggregation behavior of PM-*b*-PAA is influenced by the pH value, a series of 0.2 mg mL^{-1} dilute aqueous solutions with different pH values (pH = 2, 5, 7, 9, 12) were prepared for DLS analysis. Specifically, the hydrodynamic diameter (D_h) of $\mathbf{M_{214}A_{81}}$ in 0.2 mg mL^{-1} solution was proved to be pH-dependent. When the solution pH value increased from 2 to 9, the overall D_h decreased from 230 nm to 130 nm accompanied with more uniform particle size. This observation can be attributed to a larger value of the reduced tethering density ($\tilde{\sigma}$), which was caused by a better stretched corona with deprotonation of carboxyl groups. However, adding an excessive NaOH to the system might result in "salting-out" effect and the aggregation of crystalline micelles.[24,39] Therefore, the wide distribution and a large D_h were detected for the samples in solution with pH = 12 (**Fig. 4A**). Furthermore, identical transformation of aggregation behavior related with solution pH was also confirmed by the DLS results for $\mathbf{M_{107}A_5}$ sample (**Fig. 4B**). As exhibited, $\mathbf{M_{107}A_5}$ showed monomodal distribution with a hydrodynamic diameters of 180 nm when pH = 9, and displayed multiple size peaks at other solution pH values.

The variation of aggregation morphology as a function of pH value was obviously demonstrated by the AFM and TEM results of $\mathbf{M_{93}A_{94}}$. As seen in Fig. 5A, 5E, at a

low pH value of 2, $\mathbf{M_{93}A_{94}}$ tended to form mixture in-plane morphologies of spherical and worm-like aggregates with average width of ~120 nm. When the pH value increased to 9, $\mathbf{M_{93}A_{94}}$ aggregated into uniform disk-like micelles with diameter reducing to ~25 nm (Fig. 5C, 5G). With solution pH =12, however, large structures (up to 1 μm in one dimension) with low interfacial curvature such as cylinders and platelets formed (Fig. 5D, 5H).

The change of average size with different solution pH values could be mainly ascribed to the stretching degree of PAA corona, which was related with the ionization state in solution and could be indicated from Zeta potential (ζ) data in **Fig. S2**. Specifically, in acid solution of pH = 2, the amorphous coils collapsed and were closely covered around the crystalline core as the polymer carboxyl groups were protonated (ζ = +13.1 mV). Therefore, $\tilde{\sigma}$ become smaller and it is easy for the PM core to fuse into a larger size along the lateral surface of the PM crystal.[24] In contrast, the PAA chain would swell and fully extended in alkali solution with an increase value of $\tilde{\sigma}$. As a result, the effective negative charge repulsion from COO^- restricted the growth of crystalline core, which was similar to the effect of block composition illustrated above. When pH = 9, however, the system possessed the highest value of ζ (-46.2 mV) and tended to form a stable and monodispersed system.

3.2 The confined crystallization of PM-*b*-PAA

Despite that the aggregation behavior of PM-*b*-PAA could be facilely controlled by variables such as the block composition, it is noted from the above AFM results that the semi-crystalline platelet-like micelles cannot form a pattern with long-range order, which is also proved by using the GISAXS setup (**Fig. S3**), since there is no interference pattern in 2D GISAXS results **(Fig. S4)**. The lack of ordered, microphase-separated morphology found in PM-*b*-PAA film may result from a strong crystallization tendency of polymethylene, which is similar as the PEO-contained BCPs reported elsewhere.[42] Additionally, this random arrangement of PM-*b*-PAA micelles and polymer films on silicon substrates cannot be altered by annealing treatment (**Fig. S5**), which is usually applied on BCPs films to obtain a

pattern with long range order. And for PM-*b*-PAA micelles, this no-detectable morphological change in AFM measurements before and after thermal treatment is in accordance with other PE-containing BCPs.[35]

The experimental results of disk-like AFM morphology and the GISAXS thus demonstrated the crystalline feature of PM-*b*-PAA micelles and films. To further probe the crystallization of PM-*b*-PAA, three different types of PM-*b*-PAA were calorimetrically characterized *via* DSC measurements. The DSC results obtained from the cooling and re-heating procedures were given in **Fig.6A-B**. As can be seen, the PM-*b*-PAA bulk samples showed evident melting and crystallization peaks, which undoubtedly assigned to the crystallizable polymethylene block since polyacrylic acid is amorphous. Besides, with increasing polymethylene content from 50.53 mol % (**$M_{93}A_{94}$**) to 95.53 mol % (**$M_{107}A_5$**), the crystallization temperature (T_c) and melting point (T_m) increased from 66.3 °C to 81.6 °C, and 79.6 °C to 108.1 °C, respectively. This observation could be ascribed to the chain-folding confinement of crystallizable PM block by chemically tethered amorphous PAA block.[43] Take the comparison between **$M_{93}A_{94}$** and **$M_{107}A_5$** for example: despite the similar PM length, the free space for PM to crystallize will be reduced when a longer PAA chain is involved in **$M_{93}A_{94}$**. Hence, the crystallization and melting peaks for **$M_{93}A_{94}$** will shift to a lower temperature along with weak enthalpy change,[35] *i.e.*, the smaller integral area in DSC curves below the corresponding exothermal or endothermal peaks.

Besides in bulk samples, confined crystallization was also existed in dried PM-*b*-PAA micelles, which were prepared by vacuum freeze drying from the aqueous solution. For the XRD patterns of both **$M_{107}A_5$** and **$M_{93}A_{94}$** samples in **Fig. 6C**, the diffraction peaks located at about 21.6° and 23.8° were ascribed to the (110) and (200) reflections of the typical polyethylene orthorhombic unit cell (a = 0.741 nm, b = 0.492 nm, and c = 0.254 nm).[44] Therefore, the self-assembled aggregates comprised crystalline-confined PM core which with the identical crystallization structures as bulk polyethylene.[36] Despite the similar diffraction peak positions, the diffraction intensity was dramatically attenuated for the **$M_{93}A_{94}$** as compared to **$M_{107}A_5$**. This

phenomenon could be also explained from the interference of amorphous corona on the crystal growth of PM core in the restricted space, which resulted in a smaller PM crystal size.[45] Meanwhile, polarized optical microscope (POM) was comparatively utilized to characterize the crystalline morphology of different PM-*b*-PAA films. As indicated, the crystallization progressed more easily with larger crystal grains involved when more PM block was contained in the BCPs. Hence, this result confirmed the confined crystallization of PM-*b*-PAA, which was in well agreement with the DSC and XRD results in the aforementioned sections.

Additionally, as a potent, non-destructive tool to investigate the crystal structure of materials, GIXRD was conducted to further verify the crystalline feature of PM-*b*-PAA films. The arc crystal reflection patterns instead of oriented diffraction patterns appeared in the 2D GIXRD which clearly demonstrated the BCPs films crystallized with no preferred orientation along in-plane or out-of plane (**Fig. 7A-C**).[46] Moreover, the out-of-plane GIXRD profiles further illustrated the orthorhombic polyethylene crystalline structure, which was identical to the XRD results. Besides, a noticeable broadening of reflection peaks with increasing content of PAA in PM-*b*-PAA implied a tendency of imperfect crystallization, which mainly suffered from a confined space with PAA restriction.[43] And the reverse of relative intensity strength for $\mathbf{M_{93}A_{94}}$ suggests that the (200) crystal plane was elongated in order to accommodate carboxyl groups (-COOH) as defects in the crystal.[44]

3.3 The controlled growth of semi-crystalline PM-*b*-PAA micelles in 0.2 mg mL^{-1} DMF solution at 50 °C.

As indicated by the previous study, the semi-crystalline BCPs could also grow into a larger size, even to develop a large single crystal,[39] which makes the semi-crystalline BCPs more unique to the amorphous BCPs. Therefore, in attempt to further investigate the crystallization behavior of PM-*b*-PAA aggregates, controlled crystallization growth of the samples from dilute DMF solvent was applied for analysis. It should be pointed out that “self-seeding” method was adopted for the crystal growth in the current case,[39,47] which involved the acquirement of preformed

seed semi-crystalline micelles and their continuing growth at 50 °C. And the semi-crystalline seeds were obtained by heating the solution up to the melting point of PM (120 °C in this case) for the major melting, followed by been cooling down to the subsequent growth temperature of 50 °C for predetermined duration.

The growing size and morphology for semi-crystalline PM-*b*-PAA was traced by the AFM and TEM characterization. With the cultivation duration increasing from 0 h to 24 h, the initial elliptical micelles would follow a living growth path and developed into diamond or lozenge-like aggregates, accompanied with aggregate dimension growing from ~30 nm to ~400 nm (**Fig. 8A-C**). In addition, well-defined $\mathbf{M_{93}A_{94}}$ lozenge crystal, a typical morphology for single crystal polyethylene usually obtained in dilute solution through isothermal crystallization,[29,48] was also detected in AFM (**Fig. S7A**) and TEM observations **(Fig. 8D, Fig. S7B**). Besides, the height profiles additionally demonstrate that the well-defined $\mathbf{M_{93}A_{94}}$ lozenge crystal was almost mono-layered with a thickness of ~10 nm, which resembled that of single crystal polyethylene **(Fig. S7A)**.

Moreover, high resolution TEM (HRTEM) and selected-area electron diffraction (SAED) measurements were resorted to give a further insight of the crystalline structure of the controlled growth samples. As depicted in **Fig. 8E**, after growing for 24 h, obvious lattice fringes with *ca.* 0.37 nm interplanar spacing assigned to (200) was found inside of the $\mathbf{M_{93}A_{94}}$ aggregates. Meanwhile, the obvious contrast of crystalline core and amorphous shell further demonstrated the disk-like structure with swollen PAA tethering around the crystalline PM core.

The TEM image of $\mathbf{M_{214}A_{81}}$ aggregates grown for 24 h in **Fig. 8F** additionally illustrates that PM-*b*-PAA could grow into a large crystal lamellae. Despite the imperfect shape, the inset selected-area electron diffraction (SAED) pattern with distinct (110) and (200) diffraction spots from polyethylene crystal directly verified that PM chains adopt normal orientation to the lamella with two-dimensional folding-chain.[36] Besides, it is noteworthy that the living growth only proceeds *via* an epitaxial growth mechanism driven by crystallization of the core block, and the initial

amorphous seeds cannot bring about morphology transformation under the similar condition.[39,49,50] Therefore, the aggregation obtained by a heating and cooling step turned to function as the desired seed with a crystalline core.

Thus, considering the controlled growth of PM-*b*-PAA micelles and confined crystalline morphology evolution within different conditions, the overall scenario, mainly concerning the PM-*b*-PAA structure, such as disk-like crystalline micelles and lamellar crystal, was schematically depicted in **Fig. 9**: Prepared from coil-selective solution of DMF, PM-*b*-PAA prevailed with a disk-like morphology with crystalline PM folding as core in thickness similar as the mono-layered crystalline PE plate (~10 nm). Meanwhile, the soluble PAA, tethered to the top and bottom of the crystalline sheet, could influence the subsequent architecture of PM-*b*-PAA by retarding the chain-folding degree of PM in the confined crystallization manner. And for PM-*b*-PAA with relatively high mole fraction of PAA (*i.e.*, $\mathbf{M_{93}A_{94}}$) in moderate alkaline solution (pH = 9) or in pure DMF rather than in DMF-water binary solvents, a well-defined circular morphology in plane would be inclined. Otherwise, structure with lower curvature such as spindle-like or lamella in plane would be formed. Ultimately, under a controlled growth at 50 °C, the crystalline micelles would further grow into single crystals.

Conclusion

In summary, we have investigated the aggregation behavior and confined crystallization of PM-*b*-PAA, and further traced the controlled growth in dilute DMF solution. AFM, TEM, and DLS characterizations proved that prepared from coil-selective DMF solution, PM-*b*-PAA could form disk-like micelles with crystalline polymethylene folding as a core, which was similar with the thickness of mono-layered polyethylene crystal (~10 nm). And the aggregation behavior was controlled by block composition, solvent composition (v/v DMF/water) and solution pH value through affecting the chain-folding of PM and the stretching degree of PAA block. Furthermore, the PM-*b*-PAA bulk samples, dried micelles as well as the spin-coated films were confirmed, via DSC, WAXD and GIXRD, to possess the

confined crystallization feature of polymethylene, which was profoundly influenced by the noncrystallizable PAA block. In particularly, under the controlled growth process, crystalline PM-*b*-PAA micelles were traced to grow into single crystals even with well-defined lozenge-shaped morphology. The systematical investigation on PM-b-PAA is believed to improve the understanding of crystalline BCPs, favor the preparation of anisotropic nanostructures and afford broad application potential in block copolymers.

Acknowledgement:

GIXRD and GISAXS data were obtained at 1W1A, 1W2A, Beijing Synchrotron Radiation Facility (BSRF). The authors gratefully acknowledge the assistance of scientists from BSRF during the experiments. This work was supported by the National Natural Science Foundation of China (21072221, 21172252).

Notes and references

† Electronic supplementary information (ESI) available: Characterization and further images are included.

1. Y. Mai and A. Eisenberg, *Chem. Soc. Rev.*, 2012, **41**, 5969-5985.
2. F. H. Schacher, P. A. Rupar and I. Manners, *Angew. Chem. Int. Ed.*, 2012, **51**, 7898-7921.
3. L. F. Zhang and A. Eisenberg, *J. Am. Chem. Soc.*, 1996, **118**, 3168-3181.
4. C. M. Bates, M. J. Maher, D. W. Janes, C. J. Ellison and C. G. Willson, *Macromolecules*, 2014, **47**, 2-12.
5. E. Kaditi, G. Mountrichas, S. Pispas and C. Demetzos, *Curr. Med. Chem.*, 2012, **19**, 5088-5100.
6. I. Botiz and S. B. Darling, *Mater. Today*, 2010, **13**, 42-51.
7. Y. W. Chiang, R. M. Ho, C. Burger and H. Hasegawa, *Soft Matter*, 2011, **7**, 9797-9803.
8. R. Song, Y. Wang, X. Liu, L. He and H. Wang, *Colloids Surf., A*, 2014, **446**, 50-56.
9. L. Sun, N. Petzetakis, A. Pitto-Barry, T. L. Schiller, N. Kirby, D. J. Keddie, B. J. Boyd, R. K. O'Reilly and A. P. Dove, *Macromolecules*, 2013, **46**, 9074-9082.
10. H. Qiu, V. A. Du, M. A. Winnik and I. Manners, *J. Am. Chem. Soc.*, 2013, **135**, 17739-17742.
11. H. Schmalz, J. Schmelz, M. Drechsler, J. Yuan, A. Walther, K. Schweimer and A. M. Mihut, *Macromolecules*, 2008, **41**, 3235-3242.

12. T. Li, W. Wang, R. Liu, W. Liang, G. Zhao, Z. Li, Q. Wu and F. Zhu, *Macromolecules*, 2009, **42**, 3804-3810.
13. A. M. Mihut, J. J. Crassous, H. Schmalz, M. Drechsler and M. Ballauff, *Soft Matter*, 2012, **8**, 3163-3173.
14. Z. M. Hudson, C. E. Boott, M. E. Robinson, P. A. Rupar, M. A. Winnik and I. Manners, *Nat. chem.*, 2014, **6**, 893-898.
15. Y. Geng, P. Dalhaimer, S. Cai, R. Tsai, M. Tewari, T. Minko and D. E. Discher, *Nat. Nanotechnol.*, 2007, **2**, 249-255.
16. S. Nakagawa, K. i. Kadena, T. Ishizone, S. Nojima, T. Shimizu, K. Yamaguchi and S. Nakahama, *Macromolecules*, 2012, **45**, 1892-1900.
17. M. J. Birnkrant, C. Y. Li, L. V. Natarajan, V. P. Tondiglia, R. L. Sutherland and T. J. Bunning, *Soft Matter*, 2011, **7**, 4729-4734.
18. T. Vilgis and A. Halperin, *Macromolecules*, 1991, **24**, 2090-2095.
19. L. Yin and M. A. Hillmyer, *Macromolecules*, 2011, **44**, 3021-3028.
20. E. K. Lin and A. P. Gast, *Macromolecules*, 1996, **29**, 4432-4441.
21. J. Schmelz, M. Karg, T. Hellweg and H. Schmalz, *ACS Nano*, 2011, **5**, 9523-9534.
22. J. Schmelz, A. E. Schedl, C. Steinlein, I. Manners and H. Schmalz, *J. Am. Chem. Soc.*, 2012, **134**, 14217-14225.
23. R. Liu, Z. Li, B. Mai, Q. Wu, G. Liang, H. Gao and F. Zhu, *J. Polym. Res.*, 2013, **20**. 64.
24. W. He, J. Xu, B. Du, Z. Fan and F. Sun, *Macromol. Chem. Phys.*, 2012, **213**, 952-964.
25. A. M. Mihut, A. Chiche, M. Drechsler, H. Schmalz, E. Di Cola, G. Krausch and M. Ballauff, *Soft Matter*, 2009, **5**, 208-213.
26. J. B. Gilroy, T. Gaedt, G. R. Whittell, L. Chabanne, J. M. Mitchels, R. M. Richardson, M. A. Winnik and I. Manners, *Nat. Chem.*, 2010, **2**, 566-570.
27. A. M. Mihut, M. Drechsler, M. Moller and M. Ballauff, *Macromol. Rapid Commun.*, 2010, **31**, 449-453.
28. W. He, B. Zhou, J. Xu, B. Du and Z. Fan, *Macromolecules*, 2012, **45**, 9768-9778.
29. Y. Wang, J. Chen, S. Li, L. Li, Q. Su, J. Wang and X. Yang, *Macromolecules*, 2011, **44**, 1737-1741.
30. M. Su, H. Huang, X. Ma, Q. Wang and Z. Su, *Macromol. Rapid Commun.*, 2013, **34**, 1067-1071.
31. J. Wang, W. Zhu, B. Peng and Y. Chen, *Polymer*, 2013, **54**, 6760-6767.
32. H. Lu, Y. Xue, Q. Zhao, J. Huang, S. Xu, S. Cao and Z. Ma, *J. Polym. Sci., Part A: Polym. Chem.*, 2012, **50**, 3641-3647.
33. J. Z. Chen, K. Cui, S. Y. Zhang, P. Xie, O. L. Zhao, J. Huang, L. P. Shi, G. Y. Li and Z. Ma, *Macromol. Rapid Commun.*, 2009, **30**, 532-538.
34. J. Wang, J. H. Horton, G. Liu, S. Y. Lee and K. J. Shea, *Polymer*, 2007, **48**, 4123-4129.
35. Y. Zhao, X. Shi, H. Gao, L. Zhang, F. Zhu and Q. Wu, *J. Mater. Chem.*, 2012, **22**, 5737.

36. Z. Li, R. Liu, B. Mai, W. Wang, Q. Wu, G. Liang, H. Gao and F. Zhu, *Polymer*, 2013, **54**, 1663-1670.
37. Z. Du, J. Xu and Z. Fan, *Macromolecules*, 2007, **40**, 7633-7637.
38. Z. Du, J. Xu and Z. Fan, *Macromol. Rapid Commun.*, 2008, **29**, 467-471.
39. W. He and J. Xu, *Prog. Polym. Sci.*, 2012, **37**, 1350-1400.
40. R. F. Blanks and J. M. Prausnitz, *Ind. Eng. Chem. Fundam.*, 1964, **3**, 1-8.
41. Barton, A. F. M. CRC.*Handbook of Polymer-Liquid Interaction Parameters and Solubility Parameters*, CRC Press: Boston, 1990.
42. E. Metwalli, M. Nie, V. Koerstgens, J. Perlich, S. V. Roth and P. Mueller-Buschbaum, *Macromol. Chem. Phys.*, 2011, **212**, 1742-1750.
43. R. Liu, Z. Li, D. Yuan, C. Meng, Q. Wu and F. Zhu, *Polymer*, 2011, **52**, 356-362.
44. V. A. Kryuchkov, J.-C. Daigle, K. M. Skupov, J. P. Claverie and F. M. Winnik, *J. Am. Chem. Soc.*, 2010, **132**, 15573-15579.
45. H. K. Kim, M. Zhang, X. Yuan, S. N. Lvov and T. C. M. Chung, *Macromolecules*, 2012, **45**, 2460-2470.
46. H. Kim, S. Lee, T. J. Shin, Y. J. Cha, E. Korblova, D. M. Walba, N. A. Clark, S. B. Lee and D. K. Yoon, *Soft Matter*, 2013, **9**, 6185-6191.
47. J. Qian, Y. Lu, A. Chia, M. Zhang, P. A. Rupar, N. Gunari, G. C. Walker, G. Cambridge, F. He, G. Guerin, I. Manners and M. A. Winnik, *ACS Nano*, 2013, **7**, 3754-3766.
48. C. H. M. Weber, A. Chiche, G. Krausch, S. Rosenfeldt, M. Ballauff, L. Harnau, I. Gottker-Schnetmann, Q. Tong and S. Mecking, *Nano Lett.*, 2007, **7**, 2024-2029.
49. N. Petzetakis, A. P. Dove and R. K. O'Reilly, *Chem. Sci.*, 2011, **2**, 955-960.
50. X. Wang, G. Guerin, H. Wang, Y. Wang, I. Manners and M. A. Winnik, *Science*, 2007, **317**, 644-647.

Semi-crystalline polymethylene-*b*-poly (acrylic acid) diblock copolymers: aggregation behavior, confined crystallization and controlled growth of semicrystalline micelles from dilute DMF solution

Hongfang Wang[a], Cong Wu[a], Guangmei Xia[b], Zhi Ma[c], Guang Mo[d], Rui Song *[a]

[a]*College of Chemistry and Chemical Engineering, University of Chinese Academy of Sciences, Beijing 100049, China*

[b]*Beijing National Laboratory for Molecular Sciences, CAS Key Laboratory of Engineering Plastics, Institute of Chemistry, Chinese Academy of Sciences, Beijing 100190, China*

[c]*Shanghai Institute of Organic Chemistry, Chinese Academy of Sciences, Shanghai 200032, China*

[d]*Beijing Synchrotron Radiation Facility (BSRF), Institute of High Energy Physics, Chinese Academy of Sciences Beijing, 100049, China*

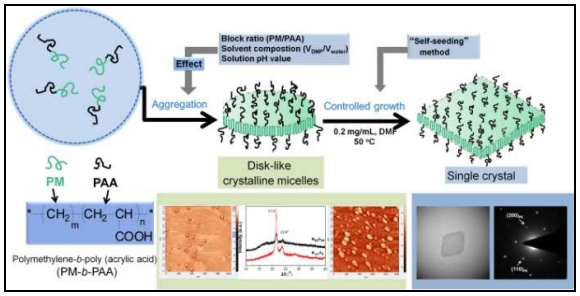

Table of contents

Systematic investigation on aggregation behavior and controlled growth of semi-crystalline polymethylene-*b*-poly (acrylic acid), which can aggregate into disk-like micelles and develop single crystals with polymethylene core being sandwiched by PAA

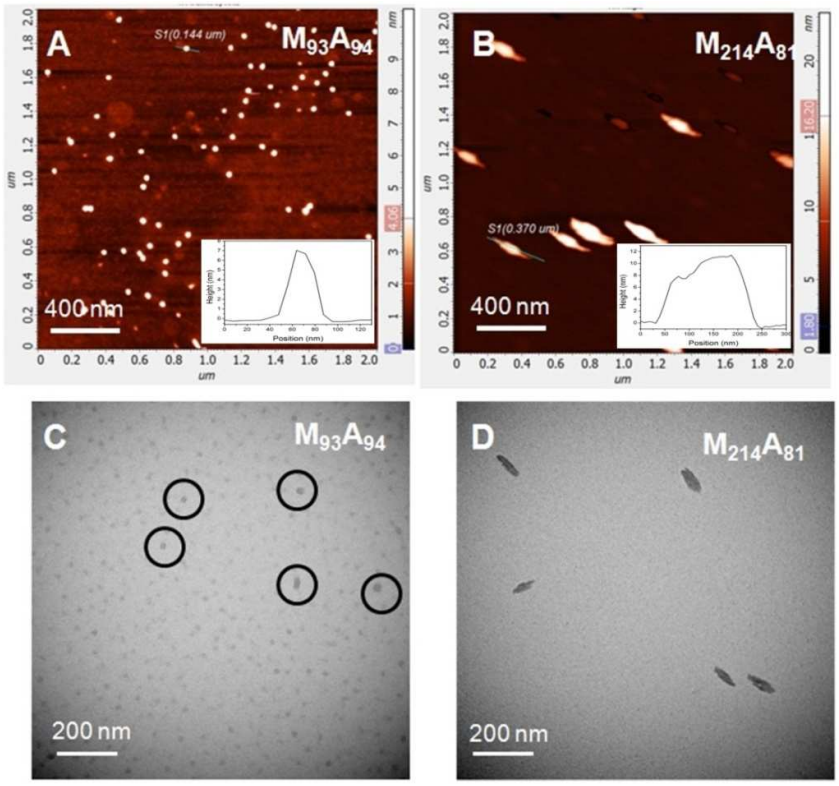

Fig. 1 AFM height images (A, B) and TEM micrographs (C, D) of PM-*b*-PAA micelles prepared from 0.2 mg mL^{-1} DMF solution. The insets are cross-section profiles of the marked positions corresponding to the height images.

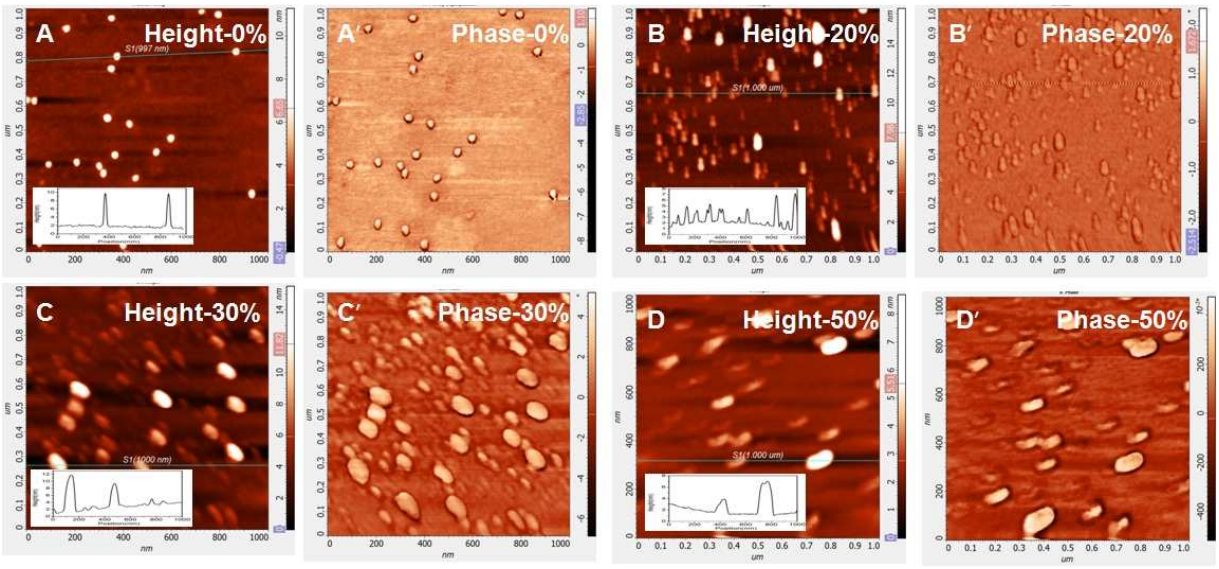

Fig. 2 AFM height (A-D) and phase images (A′-D′) (scan size: 1 um×1 um) of $\mathbf{M_{93}A_{94}}$ micelles prepared from 0.2 mg mL^{-1} solution with different DMF-water mixture solvents (x %, volume content of water). The insets are cross-section profiles of the marked positions in the corresponding height images.

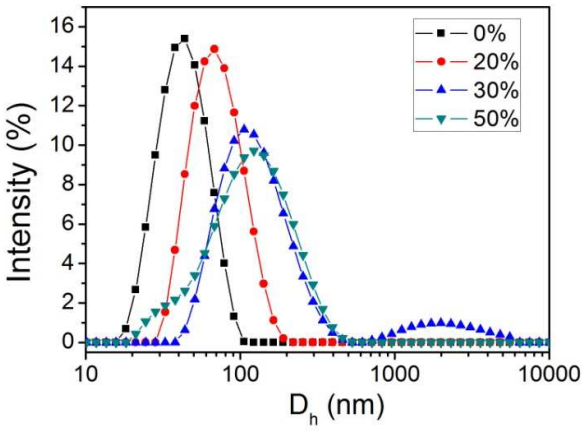

Fig. 3 Hydrodynamic diameters (D_h) of $\mathbf{M_{93}A_{94}}$ in solution (0.2 mg mL^{-1}) with different DMF-water mixture solvents (x %, volume content of water).

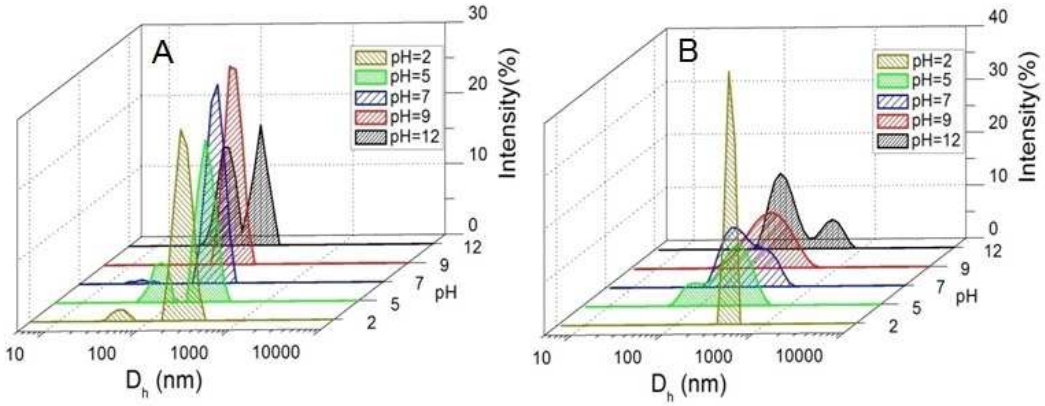

Fig. 4 Hydrodynamic diameters (D_h) of $\mathbf{M_{214}A_{81}}$ (A) and $\mathbf{M_{107}A_5}$ (B) in water (0.2 mg mL^{-1}) with different pH value of 2, 5, 7, 9, 12, respectively.

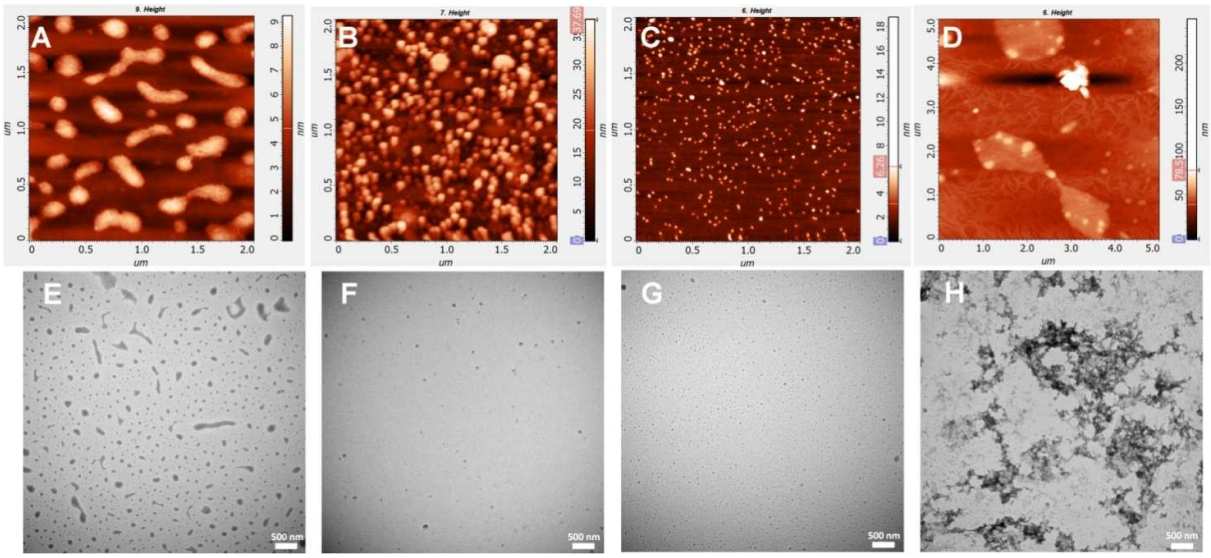

Fig. 5 AFM height images (A-D) and TEM images (E-H) of $\mathbf{M_{93}A_{94}}$ micelles prepared from 0.2 mg mL^{-1} solution with different pH values: (A, E) pH = 2, (B, F) pH = 5, (C, G) pH = 7, (D, H) pH = 12.

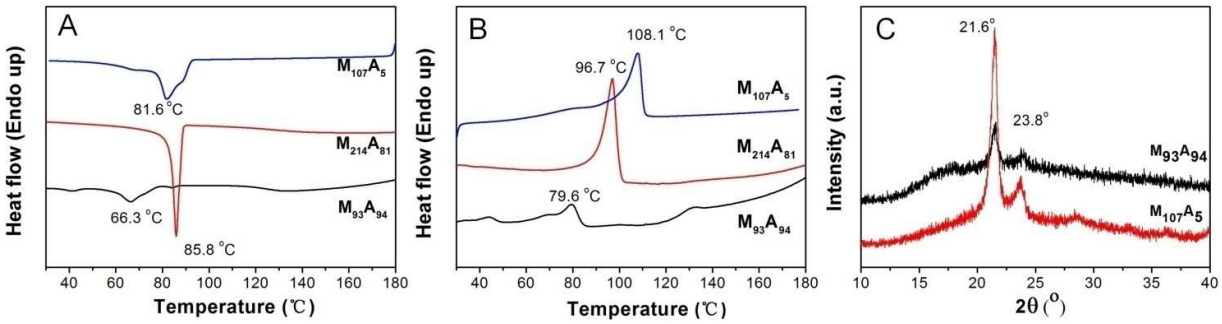

Fig. 6 DSC cooling (A) and re-heating (B) traces of PM-*b*-PAA powder; XRD patterns (C) of freeze-dried $\mathbf{M_{93}A_{94}}$ and $\mathbf{M_{107}A_5}$ samples.

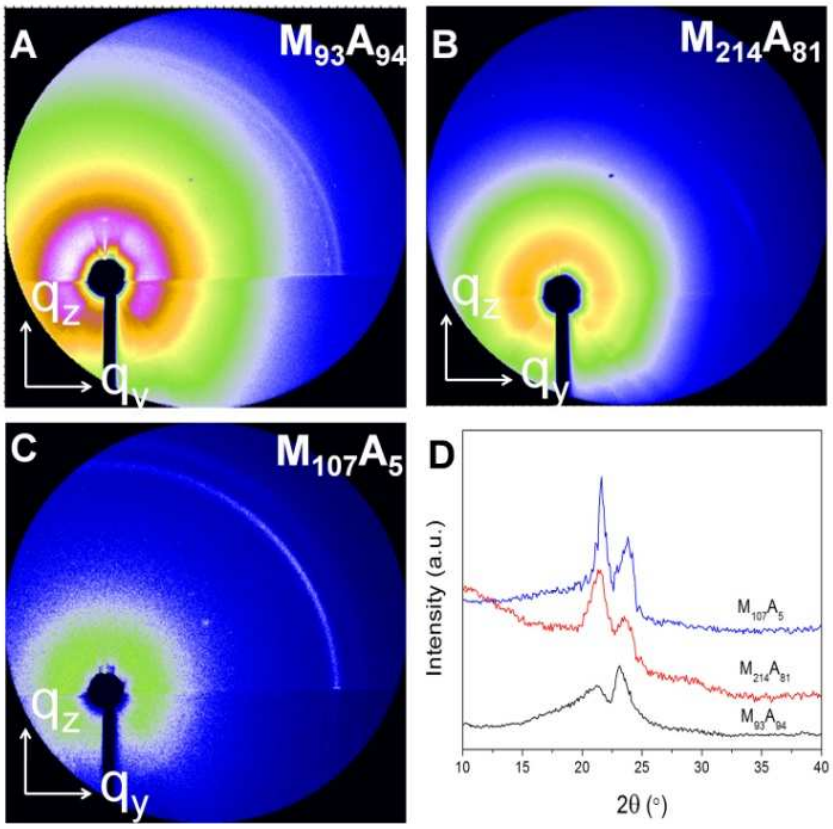

Fig. 7 Two-dimensional GIXRD patterns (2D GIXRD：A-C) and the out-of-plane XRD profiles of PM-*b*-PAA films spin-coated from 2 mg mL^{-1} DMF solution (D).

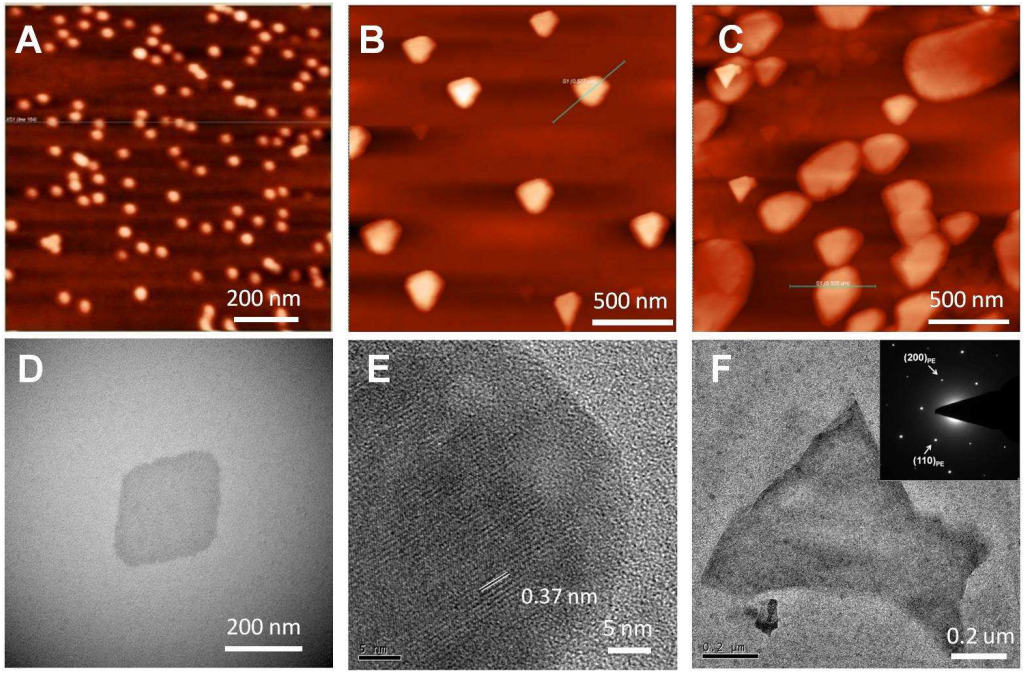

Fig. 8 AFM height images of $\mathbf{M_{93}A_{94}}$ during the controlled growth in 0.2 mg mL^{-1} dilute DMF solution for 0 h (A), 12 h (B), 24 h (C) at 50 °C; TEM micrographs of $\mathbf{M_{93}A_{94}}$ (D, E) and $\mathbf{M_{214}A_{81}}$ (F) crystals during the controlled growth from 0.2 mg mL^{-1} DMF solution for 24 h; the inset in (F) is the corresponding SAED pattern.

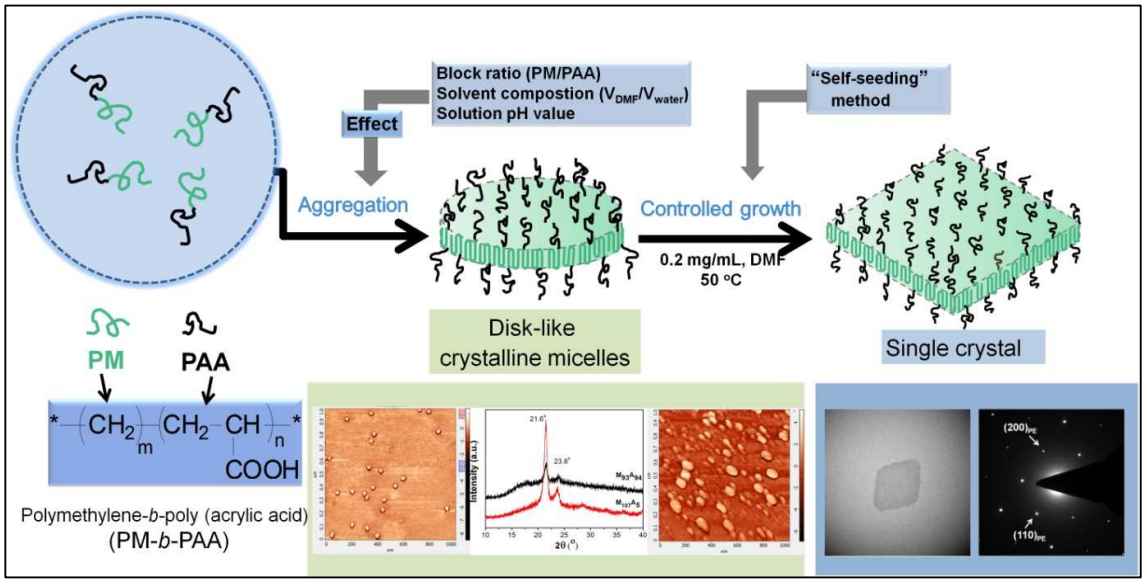

Fig. 9 Schematic representation of the aggregation behavior and the controlled growth of PM-*b*-PAA micelles with confined crystallization.